Received: 30 November 2021 | Revised: 30 September 2022 | Accepted: 8 December 2022 | IET Generation, Transmission & Distribution

DOI: 10.1049/gtd2.12730

ORIGINAL RESEARCH

Transformer-less unified power flow controller in medium voltage distribution networks

Mohamed A. Abdelrahman[1,2] | **Sheng Wang**[1] | **Wenlong Ming**[1] | **Jianzhong Wu**[1] | **Nick Jenkins**[1]

[1]School of Engineering, Cardiff University, Cardiff, UK

[2]Department of Electrical Power and Machines, Faculty of Engineering, Helwan University, Helwan, Egypt

Correspondence
Wenlong Ming, School of Engineering, Cardiff University, Cardiff, UK.
Email: MingW@cardiff.ac.uk

Funding information
Netwon-Mosharafa Fund; EPSRC Supergen Energy Networks Hub, Grant/Award Number: EP/S00078X/1

Abstract

A transformer-less unified power flow controller (UPFC) is a power electronic device consisting of series and shunt voltage source converters (VSCs) that are not connected to a common DC bus. It can control power flow in medium voltage (MV) distribution networks without the need for interfacing transformers. Hence there is a significant reduction in size and cost compared to a conventional UPFC. This paper investigates the operating range of a transformer-less UPFC in an MV distribution network and the required power ratings of the series and shunt converters. The results showed that a transformer-less UPFC is able to provide active power control using partially rated converters. However, its ability to control reactive power is limited by the current ratings of the converters. The analysis was verified using software simulation and hardware experiment.

1 | INTRODUCTION

The growth of distributed generation, energy demand and energy storage requires continuous improvements of the controllability and automation of existing medium voltage (MV) electricity distribution networks. Such improvements are possible with the increasing use of power electronic devices capable of controlling power flow. An acknowledged trend is to transfer the Flexible AC Transmission Systems (FACTs) technology to MV network applications [1, 2]. This is reflected by the commissioning of several projects which use power electronics in MV distribution networks, such as Angle-DC project ± 27 kV, 30.5 MVA [3], Flexible Power Link project 33 kV, 20 MVA [4] and Active Response project 11 kV, 5 MVA [5]. These projects aim to control the power flow (e.g. transfer excess power generated by distributed generators (DGs) to other load centres), maintain the voltages and currents within limits, improve the utilisation of existing assets, and support the growth of low carbon technologies [6, 7].

Typical MV power electronic devices for power flow control are similar to MV motor drive systems [8, 9]. Such systems consist of multi-winding line-frequency transformers with multiple three-phase voltage source converters (VSCs) that are connected back-to-back (B2B) to a common DC link [10, 11]. The B2B configuration of VSCs processes all power transfers (i.e. fully rated converters). The main advantages of a B2B configuration of VSCs are: (1) Its ability to connect busbars that might have different voltage and vector groups, and (2) it does not significantly increase the fault level of a distribution network, and it limits fault propagation [12, 13]. The main disadvantages of B2B configuration of VSCs are the high cost and size of the fully-rated VSCs and the interfacing transformers.

In order to reduce the cost and the size of power electronic devices, they can be partially rated by using series-connected VSCs, similar to the conventional Unified Power Flow Controller (UPFC) in transmission networks. Figure 1 shows a conventional UPFC composed of partially rated series and shunt converters connected through a common DC link [14]. The converters are interfaced to an AC network using series and shunt interfacing transformers. In contrast to B2B VSCs configuration, the series connection of a UPFC

offers a solution with lower rating converters and size [15]. However, a major challenge of using a conventional UPFC is the unique design characteristics of the series interfacing transformer described in [16].

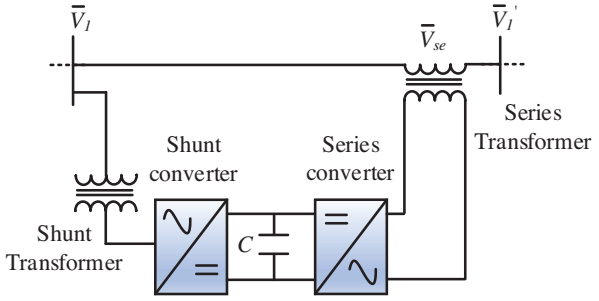

FIGURE 1 A conventional unified power flow controller

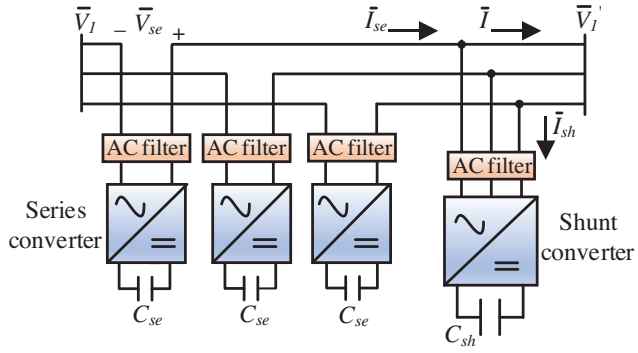

FIGURE 2 A transformer-less unified power flow controller

The size and cost of a conventional UPFC are further reduced in a transformer-less UPFC. The main advantage of a transformer-less UPFC over a conventional UPFC is the complete removal of interfacing transformers, reducing its size and cost significantly [17, 18]. Figure 2 shows the structure of a transformer-less UPFC. It has isolated series and shunt converters that are not connected to a common DC bus, similar to a STATCOM and a static series synchronous compensator (SSSC).

The converters within a transformer-less UPFC are based on cascaded H-bridge or half-bridge modules to meet the required voltage and power ratings for transmission applications [19]. By reducing the number of modules, such a device can be adapted for MV distribution networks at a low cost due to fewer semiconductor devices.

The low X/R ratio of distribution networks makes the analysis more complex than transmission networks. In addition, the main purpose of a transformer-less UPFC in a transmission network is to control active power and maintain reactive power flow to a minimal. However, this purpose might not be suitable for distribution networks, especially with the ongoing investigation to use distribution networks to provide a certain amount of controlled reactive power at grid side points (GSPs) [20, 21].

In [22], the capability of using a transformer-less UPFC to control active power in a transmission network was

tested. It was shown that the total rating of the transformer-less UPFC was reduced to half of that of a B2B configuration when the reactive power was maintained unchanged. In [23], a transformer-less UPFC was investigated to increase the transfer capability of a transmission network by connecting two separate transmission networks with a large phase difference that could not be previously connected.

Little research discussed transformer-less topologies of VSCs in MV distribution networks. Transformer-less STATCOM and SSSC were investigated to provide voltage regulation in distribution networks. A transformer-less UPFC is a hardware combination of a STATCOM and an SSSC that can be simultaneously controlled to provide power flow control in distribution networks. In [24], the performance of a 6.6 kV. 100 kVA prototype transformer-less STATCOM was investigated to manage voltage in distribution networks. The results showed the ability of the transformer-less STATCOM to provide inductive and capacitive reactive power of 100 kVAr when connected to a 6.6 kV distribution network without an interfacing transformer. In [25], a transformer-less SSSC was examined to provide voltage regulation in an 11 kV distribution network with many DGs. The results showed that the SSSC maintained the network voltage within the permissible limits by injecting a series voltage of approximately 15% of the rated network voltage. In [26, 27] the series connection of a UPFC was realised using single-phase series converters directly connected to a distribution network without an interfacing series transformer.

Further investigation is required to assess the ability of a transformer-less UPFC to control both active and reactive power in distribution networks and the size of the series and shunt converters. This paper investigates the operation of a transformer-less UPFC in an MV distribution network with a low X/R ratio. It provides a detailed analysis of the operating range of a transformer-less UPFC considering both active and reactive power control. It also examines the magnitude of the shunt current required to change the power flow from various uncompensated active and reactive power to an arbitrary target active and reactive power. It highlights that the magnitude of the shunt current and, therefore, the ratings of the converters are small when a transformer-less UPFC is used to control active power. However, a transformer-less UPFC has limited capability to control reactive power due to the current ratings of the converters. The analysis was verified using simulation and a small-scale experimental setup.

2 | TRANSFORMER-LESS UPFC IN AN MV DISTRIBUTION NETWORK

Figure 3 shows the equivalent circuit of a transformer-less UPFC connected in a two-busbar distribution network. The series converter is modelled as a controlled voltage source and the shunt converter as a controlled current source.

The voltage and current at busbar $\overline{V}_1'$ are given as:

$$\begin{cases} \overline{V}_1' = \overline{V}_1 + \overline{V}_{se} \\ \bar{I}_{se} = \bar{I} + \bar{I}_{sh} \end{cases} \quad (1)$$

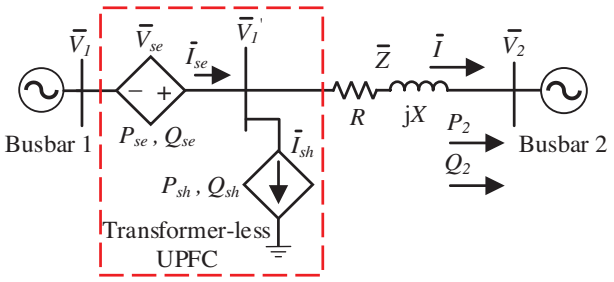

FIGURE 3 Equivalent circuit of a transformer-less UPFC connected to a two-busbar distribution network

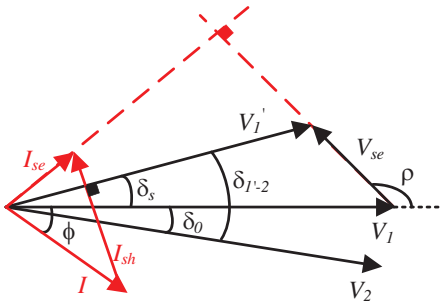

FIGURE 4 The basic principle of a transformer-less UPFC

Figure 4 shows a phasor diagram developed using the equivalent circuit in Figure 3. It explains the role of the series and shunt converters, where voltage $\overline{V}_1$ of Busbar 1 is taken as a reference and δ_0 represents the power angle between $\overline{V}_1$ and voltage $\overline{V}_2$ of Busbar 2.

The role of the series converter in a transformer-less UPFC is similar to that in a conventional UPFC. It injects a controllable voltage $\overline{V}_{se} = |\overline{V}_{se}|\angle\rho$. This voltage is added to $\overline{V}_1$ making the resultant voltage $\overline{V}'_1 = |\overline{V}'_1|\angle\delta_s$ whose magnitude and power angle are regulated to achieve the target active and reactive power P_2 and Q_2 as shown by the voltage phasors in Figure 4.

The role of the shunt converter in a transformer-less UPFC is different from that in a conventional UPFC. The shunt converter ensures zero active power exchange between both the converters within a transformer-less UPFC and the connected AC network (i.e. $P_{se} = 0$ and $P_{sh} = 0$). To achieve this, the shunt current $\overline{I}_{sh}$ is controlled to be perpendicular to $\overline{V}'_1$ (i.e. $\overline{I}_{sh} \perp \overline{V}'_1$), and it must make the series current $\overline{I}_{se}$ perpendicular to $\overline{V}_{se}$ (i.e. $\overline{I}_{se} \perp \overline{V}_{se}$) as shown by the current phasor in Figure 4.

The distribution feeder is represented by a series impedance $\overline{Z} = |\overline{Z}|\angle\theta$. The current through the distribution feeder can be obtained as $\overline{I} = (\overline{V}'_1 - \overline{V}_2)/|\overline{Z}|\ \angle\theta$. Therefore, the apparent power $\overline{S}_2$ at Busbar 2 is given as in (2).

$$\overline{S}_2 = \overline{V}_2 \cdot \overline{I}^* = \overline{V}_2 \cdot \left(\frac{\overline{V}'_1 - \overline{V}_2}{|\overline{Z}|\ \angle\theta}\right)^* = P_2 + j\,Q_2 \quad (2)$$

The active and reactive power P_2 and Q_2 are given, as in (3).

$$\begin{cases} P_2 = \underbrace{\dfrac{|\bar{V}_1| \cdot |\bar{V}_2|}{|\bar{Z}|}\cos(\delta_0 + \theta) - \dfrac{|\bar{V}_2|^2}{|\bar{Z}|}\cos\theta}_{\textit{Uncompensated active power}} \\ \qquad + \underbrace{\dfrac{|\bar{V}_2| \cdot |\bar{V}_{se}|}{|\bar{Z}|}\cos(\delta_0 + \theta - \rho)}_{\textit{Controllable active power}} \\ Q_2 = \underbrace{\dfrac{|\bar{V}_1| \cdot |\bar{V}_2|}{|\bar{Z}|}\sin(\delta_0 + \theta) - \dfrac{|\bar{V}_2|^2}{|\bar{Z}|}\sin\theta}_{\textit{Uncompensated reactive power}} \\ \qquad + \underbrace{\dfrac{|\bar{V}_2| \cdot |\bar{V}_{se}|}{|\bar{Z}|}\sin(\delta_0 + \theta - \rho)}_{\textit{Controllable reactive power}} \end{cases} \quad (3)$$

Equation (3) shows that $\overline{V}_{se}$ affects both P_2 and Q_2. However, if the transformer-less UPFC is deactivated (i.e. $\overline{V}_{se} = 0$), the uncompensated active and reactive power P_2' and Q_2' are given, as in (4).

$$\begin{cases} P_2' = \dfrac{|\overline{V}_1| \cdot |\overline{V}_2|}{|\overline{Z}|}\cos(\delta_0 + \theta) - \dfrac{|\overline{V}_2|^2}{|\overline{Z}|}\cos\theta \\ Q_2' = \dfrac{|\overline{V}_1| \cdot |\overline{V}_2|}{|\overline{Z}|}\sin(\delta_0 + \theta) - \dfrac{|\overline{V}_2|^2}{|\overline{Z}|}\sin\theta \end{cases} \quad (4)$$

The difference between (3) and (4) is the controllable active and reactive power P_c and Q_c of a transformer-less UPFC (i.e. $P_c = P_2 - P_2'$ and $Q_c = Q_2 - Q_2'$), and are given as in (5).

$$\begin{cases} P_c = \dfrac{|\overline{V}_2| \cdot |\overline{V}_{se}|}{|\overline{Z}|}\cos(\delta_0 + \theta - \rho) \\ Q_c = \dfrac{|\overline{V}_2| \cdot |\overline{V}_{se}|}{|\overline{Z}|}\sin(\delta_0 + \theta - \rho) \end{cases} \quad (5)$$

By further simplifying (5) yields the expression of $\overline{V}_{se}$ as given in (6).

$$|\overline{V}_{se}| = \frac{|\overline{Z}|}{|\overline{V}_2|}\sqrt{P_c^2 + Q_c^2},\ \rho = (\delta_0 + \theta - \tan^{-1}(\frac{Q_c}{P_c})) \quad (6)$$

Equation (6) shows that $|\overline{V}_{se}|$ is a function of $|\overline{Z}|$, P_c, Q_c and $|\overline{V}_2|$.

The current at busbar $\overline{V}_1{}'$ is obtained as in (7), where ϕ is the angle between $\overline{V}_1$ and $\overline{I}$. Note that the series current $\overline{I}_{se}$ is the resultant of the shunt current and the current of the distribution feeder (i.e. $\overline{I}_{se} = \overline{I}_{sh} + \overline{I}$).

$$\left|\overline{I}_{sh}\right| \angle(\delta_s + 90°) = \left|\overline{I}_{se}\right| \angle(\rho - 90°) - \left|\overline{I}\right| \angle\phi \tag{7}$$

Equation (7) is used to obtain an expression of $\overline{I}_{sh}$, as in (8). Detailed derivation of (8) is provided in the Appendix.

$$\overline{I}_{sh} = \left|\overline{I}\right| \cdot \frac{\cos(\rho - \phi)}{\sin(\rho - \delta_s)} \angle(\delta_s - 90)° \tag{8}$$

Equations (6), and (8) are used to calculate the reference voltage and current $\overline{V}_{se}{}^*$ and $\overline{I}_{sh}{}^*$ for the series and shunt converters. As the feeder's impedance is known, a transformer-less UPFC relies on the measurements of $\overline{V}_1$, $\overline{V}_2$ and $\overline{I}$ to calculate its $\overline{V}_{se}{}^*$ and $\overline{I}_{sh}{}^*$. $\overline{V}_1$ is measured locally, while $\overline{V}_2$ requires communication.

3 | OPERATING RANGE OF A TRANSFORMER-LESS UPFC IN MV DISTRIBUTION NETWORKS

The operating range of a transformer-less UPFC was investigated based on the modelling conducted in Section 2. It describes the capability of a transformer-less UPFC to control active and reactive power in an MV distribution network, and it is directly related to the power ratings of the series and shunt converters.

The series and the shunt converters' power ratings must fulfil the maximum apparent power $|\overline{S}_{se}|$ and $|\overline{S}_{sh}|$ exchanged between the converters and the connected AC network (i.e. $|\overline{V}_{se}| \cdot |\overline{I}_{se}| \le |\overline{S}_{se}|$& $|\overline{V}_1{}'| \cdot |\overline{I}_{sh}| \le |\overline{S}_{sh}|$).

3.1 | Series converter

The power rating of the series converter is estimated by calculating $|\overline{V}_{se}|$ using (6). Note that $|\overline{V}_{se}|$ is advantageously smaller in MV distribution networks than in transmission networks due to the smaller impedance. Assuming $|\overline{V}_2|$ is 0.95 p.u., the term $\sqrt{P_c^2 + Q_c^2}$ is 2.0 p.u. (e.g. the series converter can reverse the active power from 1.0 to −1.0 p.u., while the reactive power was maintained to zero) and impedance $|\overline{Z}|$ ranges between 5% to 10%, then the range of $|\overline{V}_{se}|$ is calculated to be between 0.105 to 0.210 p.u. As current $|\overline{I}_{se}|$ is 1.0 p.u., the power rating of the series converter also ranges between 0.105 to 0.210 p.u.

3.2 | Shunt converter

The shunt converter has full network voltage applied across its terminal. The power rating of the shunt converter is determined based on $|\overline{I}_{sh}|$. Therefore, it is required to calculate the maximum shunt current required to ensure zero active power exchange between each of the series and shunt converters and the connected AC network.

An algorithm was developed to calculate the shunt current as shown in Figure 5. It calculates $|\overline{I}_{sh}|$ when the power flow changes from various uncompensated active and reactive $P_2{}'$ and $Q_2{}'$ (i.e. prior to connecting the transformer-less UPFC) to an arbitrary target active and reactive power P_2 and Q_2.

Firstly, various operating conditions of $P_2{}'$ and $Q_2{}'$ are generated by hypothetically changing $|\overline{V}_2|$ and δ_2, while maintaining $|\overline{V}_1|$ and δ_1 constant at 1.0∠0° p.u. Busbar 1 was taken as a stiff busbar to demonstrate the inherent capability of a transformer-less UPFC. Note that a non-stiff busbar adds further limitations on the operating range of the transformer-less UPFC. For example, an increase in voltage at the point of connection reduces the reactive power the shunt converter can supply.$P_2{}'$ and $Q_2{}'$ are calculated using (4), and are stored in matrices $[P_2{}']_{M\times N}$ and $[Q_2{}']_{M\times N}$where M and N are the range of $|\overline{V}_2|$ and δ_2. For example, $|\overline{V}_2|$ is changed from 0.95 to 1.03 p.u. and δ_2 from −5° to +5° such as $\sqrt{(P_2{}')^2 + (Q_2{}')^2} \le S_2$ where S_2 is the nominal apparent power of the distribution feeder.

Secondly, an arbitrary target power P_2 and Q_2 is chosen such as $\sqrt{(P_2)^2 + (Q_2)^2} \le S_2$. Thirdly, voltage $[\overline{V}_{se}]_{M\times N}$, current $[\overline{I}_{sh}]_{M\times N}$ and current $[\overline{I}_{se}]_{M\times N}$ are calculated using (6)–(8). Finally, the algorithm checks the current constraints (i.e. $|\overline{I}_{sh}|$&$|\overline{I}|$&$|\overline{I}_{se}| \le 1.0$ p.u.).

Figure 6 shows the mapping of $|\overline{I}_{sh}|$ against $P_2{}'$ and $Q_2{}'$. The base apparent power and voltage were 10 MVA and 12.66 kV. The impedance of the distribution feeder was 8%, and the X/R was 2.0. A circle of 1.0 p.u. radius represents all the values of $P_2{}'$ and $Q_2{}'$. The colour map provides the shunt current's magnitude at every power $P_2{}'$ and $Q_2{}'$ to the target power of (0.6 p.u., 0.2 p.u.) such as, dark blue area represents zero shunt current, while dark red area represents 1.0 p.u. shunt current. The areas with black circles and red crosses are inoperable as either $|\overline{I}_{sh}|$ and $|\overline{I}_{se}|$ exceeded 1.0 p.u. or $|\overline{I}_{se}|$ exceeded 1.0 p.u.

Three cases were selected to demonstrate the shunt current's magnitude by changing the uncompensated power "A", "B" and "C" to the same target power. These cases are:

Case A: The change of power flow from A (0.2 p.u., 0.2 p.u.) to target power (0.6 p.u., 0.2 p.u.), where the per-unit values in each bracket are the active and reactive power.

Case B: The change of power flow from B (0.6 p.u., 0 p.u.) to target power (0.6 p.u., 0.2 p.u.).

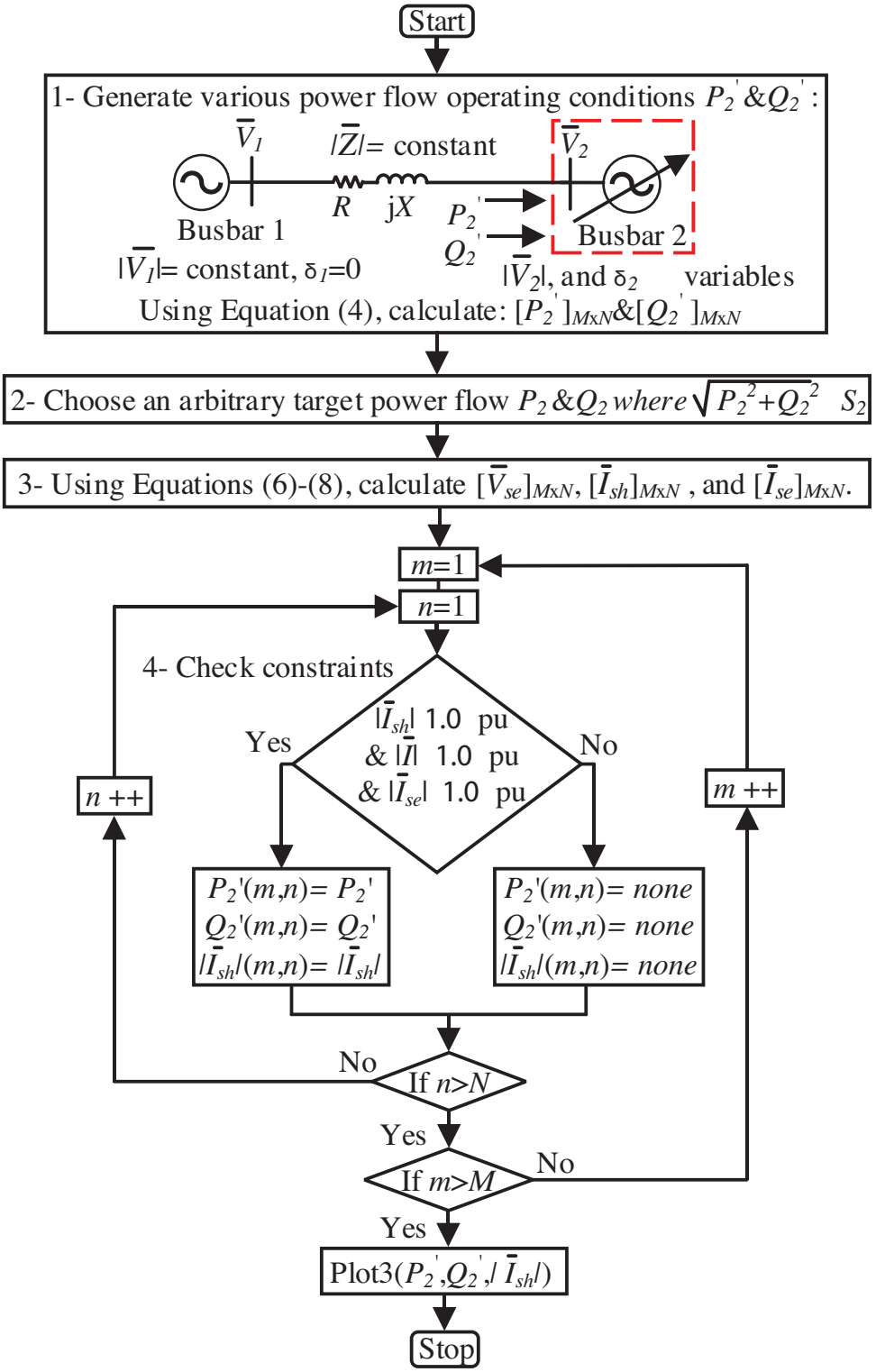

FIGURE 5 The algorithm used to determine the shunt current

Case C: The change of power flow from C (0.2 p.u., 0 p.u.) to target power (0.6 p.u., 0.2 p.u.).

It can be observed that in case A, $|\bar{I}_{sh}|$ was only 0.1 p.u. when the power flow changed from A to the target power (i.e. step change of active power from 0.2 to 0.6 p.u., while the reactive power was maintained constant). In case B, the change of power flow from B to the target power (i.e. step change of reactive power from 0 to 0.2 p.u. while the active power was maintained constant) was in the area with black circles as $|\bar{I}_{sh}|$and$|\bar{I}_{se}|$ exceeded 1.0 p.u. In case C, the change of

TABLE 1 Voltage and current of the series and shunt converters (Bold values denote the currents exceeded 1.0 p.u.)

Point	Series voltage $\bar{V}_{se}$ (p.u.)	Series current $\bar{I}_{se}$ (p.u.)	Voltage $\overline{V}'_1$ (p.u.)	Shunt current $\bar{I}_{sh}$ (p.u.)
B→Target Power (0.6 pu, 0.2 pu)	$0.016\angle -29°$	$\mathbf{1.26}\angle 61°$	$1.014\angle -0.5°$	$\mathbf{1.33}\angle 89.5°$
C→Target Power (0.6 pu, 0.2 pu)	$0.035\angle 37°$	$\mathbf{1.03}\angle -53°$	$1.03\angle 1.2°$	$0.61\angle -88.8°$

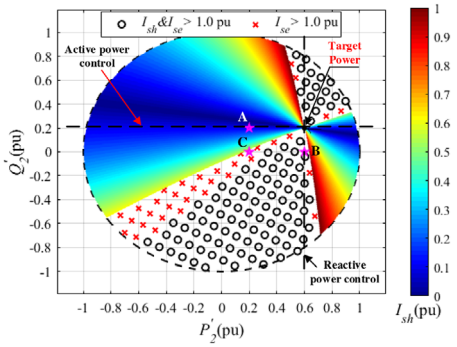

FIGURE 6 Mapping of shunt current against P_2' and Q_2' for cases A, B and C

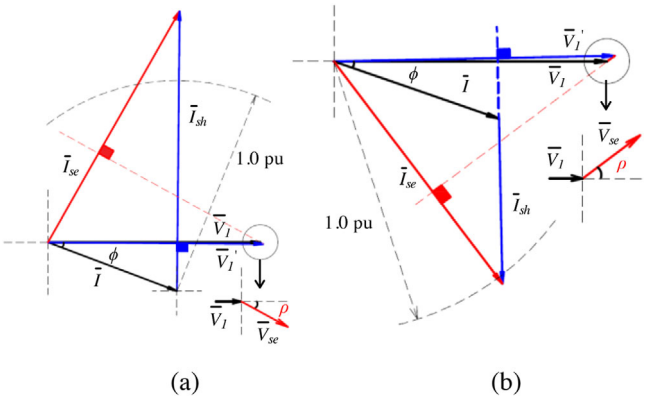

FIGURE 7 Scaled phasor diagrams; (a) $|\bar{I}_{sh}|$and$|\bar{I}_{se}|$ > p.u., and (b) $|\bar{I}_{se}|$ > p.u.

power flow from C to the target power (i.e. step change of active power from 0.2 to 0.6 p.u. and reactive power from 0 to 0.2 p.u.) was in the area with red crosses as $|\bar{I}_{se}|$ exceeded 1.0 p.u.

Note that in all cases, the power flow was changed from either "A", "B" or "C" to "Target Power" by injecting the corresponding series voltage $\overline{V}_{se}$. While $|\bar{I}_{sh}|$ is required to guarantee zero active power exchange between each of the series and shunt converters and the connected AC network.

A horizontal line labelled as "Active power control" was drawn to the target power where P_2' changes while Q_2' is constant (i.e. active power control). The points along the horizontal line show a maximum shunt current's magnitude of 0.1 p.u. This demonstrates the ability of the transformer-less UPFC to control active power using a small shunt current. Similarly, a vertical line labelled as "Reactive power control" was drawn to the target power where Q_2' changes while P_2' is constant (i.e. reactive power control). The vertical line is entirely in the areas with red crosses and black circles, hence the transformer-less UPFC is inoperable.

Table 1 shows steady-state voltages and currents of the series and shunt converters for Case B and Case C when the transformer-less UPFC was inoperable. These values were calculated using (1), (6) and (7). Figure 7 shows scaled phasor diagrams developed using Table 1 where cases B and C are inoperable due to current constraints.

3.3 | Shunt current for several target power

Figure 8 shows $|\bar{I}_{sh}|$ against P_2' and Q_2' for several target power points. Figure 8a–c shows similar characteristics when the target power was changed to several arbitrary points in the four-quadrant of operation. In this case, $|\bar{I}_{sh}|$ has a maximum value of 0.5 p.u. for active power control (see green area in Figures 8a and 8c), while either $|\bar{I}_{sh}|$ and $|\bar{I}_{se}|$ exceeded 1.0 p.u. or $|\bar{I}_{se}|$ exceeded 1.0 p.u. for reactive power control.

3.4 | Analysis of the shunt current

Simplified expressions of $|\bar{I}_{sh}|$ obtained in two cases:

(1) Active power control (i.e. $Q_c = 0$), and (2) reactive power control (i.e. $P_c = 0$).

Firstly, an approximate expression of $|\bar{I}_{sh}|$ can be obtained from (8) by neglecting angle δ_s which is usually small in MV distribution networks, as in (9).

$$\left|\bar{I}_{sh}\right| = \left|\bar{I}\right| \cdot \left(\frac{\cos(\phi)}{\tan(\rho)} + \sin(\phi)\right) \tag{9}$$

Secondly, approximate expressions of P_c and Q_c can be obtained from (5) by neglecting the angle δ_0, as in (10),

where V_d and V_q are the direct and quadrature components of $\overline{V}_{se}$.

$$\begin{cases} P_c \cong \dfrac{V_2 R}{Z^2} V_d + \dfrac{V_2 X}{Z^2} V_q \\ Q_c \cong \dfrac{V_2 X}{Z^2} V_d - \dfrac{V_2 R}{Z^2} V_q \end{cases} \tag{10}$$

When $Q_c = 0$, then substituting in (10) obtains $V_q/V_d = X/R$ or $\tan(\rho) = X/R$. In this case, $|\bar{I}_{sh}|$ can be approximately

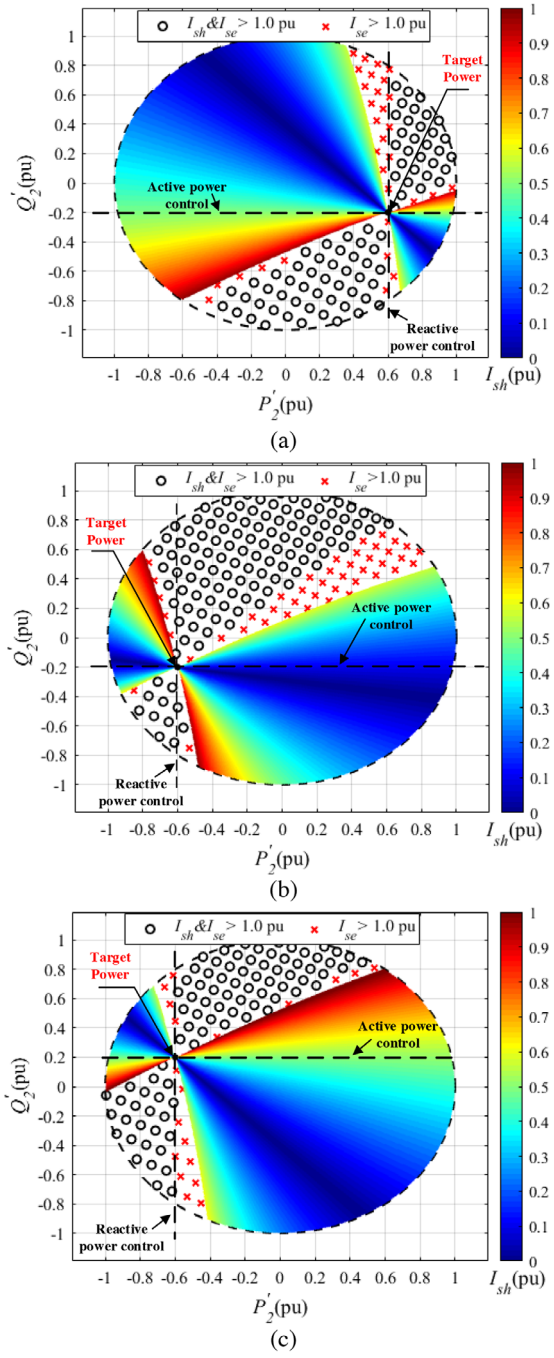

FIGURE 8 Shunt current's magnitude mapped against P_2' and Q_2' for several target power; (a) A (0.6 p.u., −0.2 p.u.), (b) A (−0.6 p.u., −0.2 p.u.) and (c) A (−0.6 p.u., 0.2 p.u.)

rewritten, as in (11).

$$\left|\bar{I}_{sh}\right| \approx \left|\bar{I}\right| \cdot \left(\frac{\cos(\phi)}{X/R.} + \sin(\phi)\right) \tag{11}$$

The feeder is utilised for active power control, and so ϕ is close to zero. Therefore, $|\bar{I}_{sh}|$ is a fraction of $|\bar{I}|$ considering a distribution feeder of an X/R greater than 1.0.

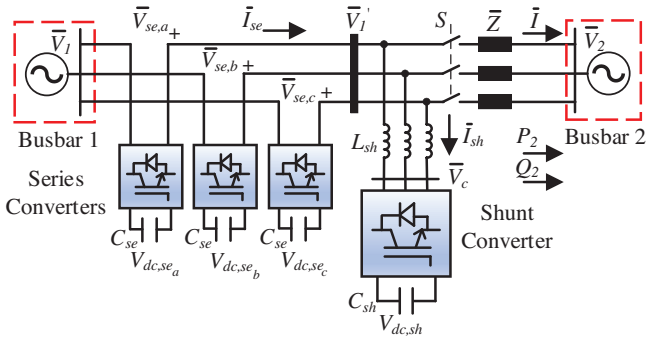

FIGURE 9 Simulated transformer-less UPFC

Similarly, when $P_c = 0$, then substituting in (10) obtains $V_q/V_d = -R/X$. In this case, $|\bar{I}_{sh}|$ can be rewritten, as in (12).

$$\left|\bar{I}_{sh}\right| \approx \left|\bar{I}\right| \cdot \left(\frac{\cos(\phi)}{R/X} + \sin(\phi)\right) \tag{12}$$

Equation (12) demonstrates that $|\bar{I}_{sh}|$ is very likely to exceed 1.0 p.u. especially as the X/R ratio of a distribution feeder increases.

The above analysis demonstrates that a transformer-less UPFC can control active power with a partially rated shunt converter. Equations (11) and (12) show that various values of feeder's X/R ratio will affect the shunt current magnitudes, consequently the operating range of a transformer-less UPFC.

Assume a full-load operation of $|\bar{I}|$, ϕ is zero and the X/R ratio is 2.0, using (11), the power rating of the shunt converter is 0.5 p.u. when used to control active power. Note that the rating of the series converter is 10–20% of the nominal apparent power, as given in Section 3.1. The ability of a transformer-less UPFC to control reactive power is limited by the converters' current ratings.

4 | SIMULATION STUDY

4.1 | Control scheme of the simulated transformer-less UPFC

Figure 9 shows the test system implemented in MATLAB Simulink to validate the theoretical analysis in Section 3. A transformer-less UPFC was connected to a 10 MVA, 12.66 kV distribution feeder whose impedance was 8%, X/R ratio of 2. The base apparent power and voltage were 10 MVA and 12.66 kV. The series converters were implemented using single-phase two-level VSCs, while the shunt converter was implemented using a three-phase, two-level VSC. The DC-link capacitance of the series and shunt converters are 12 mF and 0.5 mF and were calculated from $C_{se} \geq \frac{S_{se}}{\omega\, V_{dc,se}\, \Delta V_{dc}}$ and $C_{sh} \geq \frac{S_{sh}}{2\,\omega\, V_{dc,sh}\, \Delta V_{dc}}$, where ΔV_{dc} is the ripple component of the DC voltage [29, 30]. Selection criteria for the DC-link capacitors can be found in [31]. The parameters of the transformer-less UPFC model are summarised in Table 2.

TABLE 2 Parameters of the transformer-less UPFC model

	Parameter	Value
Series converter	Nominal power, S_{se}	1.5 MVA
	DC voltage, $V_{dc,se}$	1750 V
	DC capacitance, C_{se}	12 mF
Shunt converter	Nominal power, S_{sh}	10 MVA
	DC voltage, $V_{dc,sh}$	30 kV
	DC capacitance, C_{sh}	0.5 mF
	Filter inductance, L_{sh}	20 mH

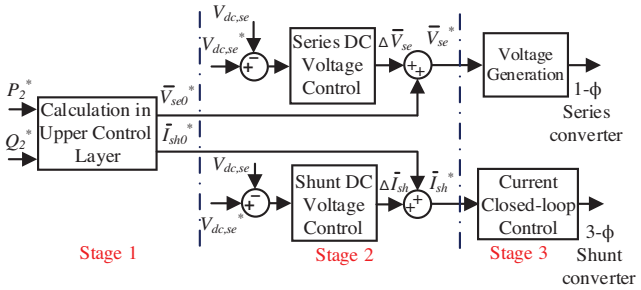

FIGURE 10 Overall control scheme of a transformer-less UPFC [28]

4.1.1 | Overall control

The transformer-less UPFC was operated to control active and reactive power P_2 and Q_2 at Busbar 2 independently. Figure 10 shows the overall control structure [28]. In stage 1, the desired active and reactive power at Busbar 2 P_2^* and Q_2^* were used to calculate the reference voltage $\bar{V}_{se0}^*$ of the series converter and the reference current $\bar{I}_{sh0}^*$ of the shunt converter according to (6) and (8). When $\bar{V}_{se}$ and $\bar{I}_{sh}$ are regulated effectively, P_2 and Q_2 will be maintained close to P_2^* and Q_2^*. In stage 2, the DC voltage control loops of the series and shunt converters are found. Their outputs are $\Delta\bar{V}_{se}$ and $\Delta\bar{I}_{sh}$ which are added to $\bar{V}_{se0}^*$ and $\bar{I}_{sh0}^*$. In stage 3, the series and shunt converters generate the switching signals of the IGBTs.

4.1.2 | Individual control of the series converter

Figure 11 shows the control loop of the single-phase series converter.

In total, three identical control loops were used for the series converters.

The DC voltage controller (in the red dash box) maintains the DC voltage $V_{dc,se}$ of the series converter at its reference value $V_{dc,se}^*$. The PI controller eliminates the error between $V_{dc,se}$ and $V_{dc,se}^*$ and generates an output power P_{se} which equals the power losses of the converter (i.e. $P_{se} = P_{loss}$). This ensures the active power is balanced within the converter. The output P_{se} is then divided by I_{se}^2 to obtain a virtual resistance R_{se} that is equal to the equivalent resistance of the converter. R_{se} is further mul-

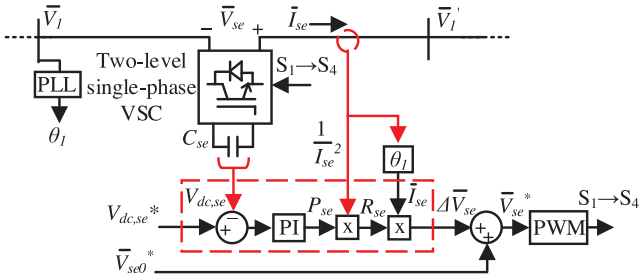

FIGURE 11 Control scheme of the single-phase series converter

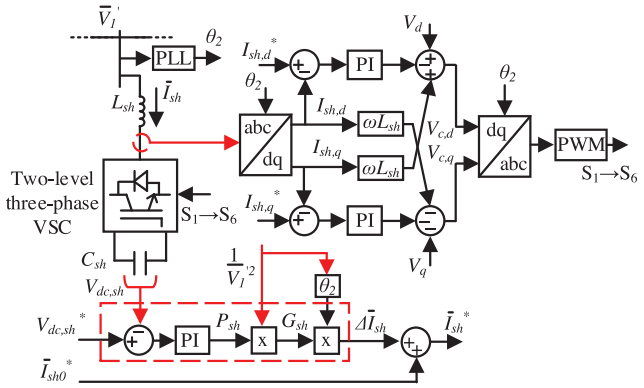

FIGURE 12 Control scheme of the three-phase shunt converter

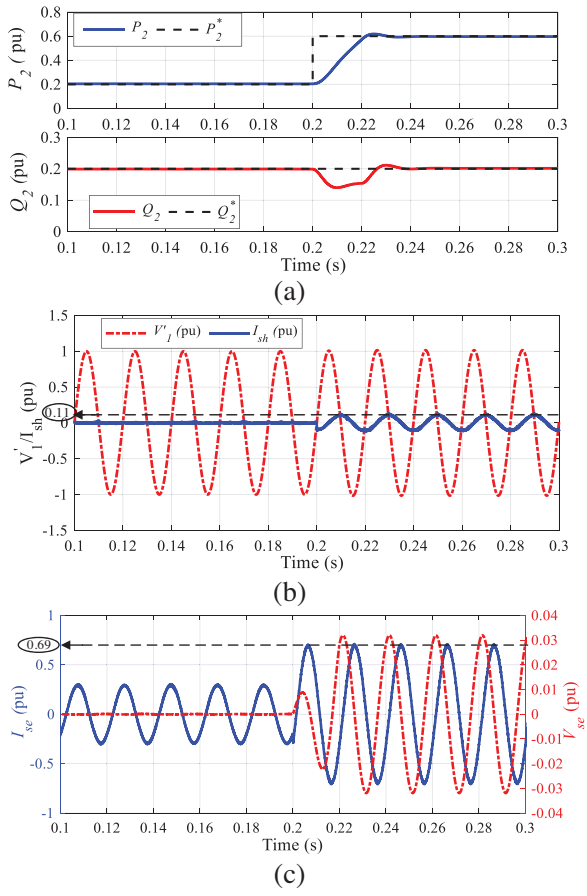

FIGURE 13 Simulation waveforms of case A; (a) P_2 and Q_2, (b) $\overline{V}_1'$ and $\overline{I}_{sh}$ and (c) $\overline{V}_{se}$ and $\overline{I}_{se}$

tiplied by the vector $\bar{I}_{se}$ to obtain the AC voltage drop across the converter ΔV_{se} caused by the equivalent resistance of the converter. ΔV_{se} needs to be added to $\bar{V}^*_{se0}$ to compensate for the AC voltage drop. The sum $\bar{V}^*_{se0} + \Delta V_{se}$ is the reference voltage $\bar{V}^*_{se}$ that is forwarded to the PWM block, generating the switching signals ($S_1 \rightarrow S_4$).

4.1.3 | Individual control of the shunt converter

Figure 12 shows the current control loops of the three-phase shunt converter. The DC voltage controller (in the red dash box) maintains the DC voltage $V_{dc,sh}$ of the shunt converter at its reference value $V_{dc,sh}{}^*$. It has similar control structure to the DC voltage controller of the series converter.

The shunt current is regulated in the *dq* frame using *abc* to *dq* transformation. The *dq* current errors ($I_{sh,d}{}^* - I_{sh,d}$) and ($I_{sh,q}{}^* - I_{sh,q}$) are sent to the PI controllers of the current control loops [32]. The PI controllers minimise the *dq* current errors and generate the reference *dq* voltage signals $V_{c,d}$ and $V_{c,q}$, which are then transformed into *abc* frame using *dq* to

abc transformation. The PWM block generates the gate signals of the IGBTs ($S_1 \rightarrow S_6$).

4.2 | Simulation results

The same three cases (Case A, Case B and Case C) shown in Figure 6 were simulated.

4.2.1 | Case A

Figure 13 shows the voltages and currents of the series and shunt converters when a step change of active power occurred at $t = 0.2$ s in response to a change in active power control signal. Before $t = 0.2$ s, the uncompensated active power was 0.2 p.u. and the uncompensated reactive power was 0.2 p.u.

Figure 13a shows that P_2 was increased from 0.2 to 0.6*p.u.* while $Q_2$was maintained unchanged at 0.2 p.u. in steady state. This demonstrates the ability of the transformer-less UPFC to independently control the active and reactive power.

Figures 13b and 13c show that after $t = 0.2$ s, currents $|\bar{I}_{sh}|$ and $|\bar{I}_{se}|$ were 0.11 and 0.69 p.u. and both were 90°phase shift w.r.t. voltages $\bar{V}_1'$ and $\bar{V}_{se}$. This small shunt current matches with the analysis in Section 3 (i.e. Case A). Thus, it demonstrates the ability of the transformer-less UPFC to regulate active power with a small requirement of shunt current (i.e. partially rated shunt converter).

4.2.2 | Case B

Figure 14 shows the voltages and currents of the series and shunt converters when a step change of reactive power occurred at $t = 0.2$ s in response to a change in reactive power control signal. Before $t = 0.2$ s, the uncompensated active power was 0.6 p.u. and the uncompensated reactive power was zero.

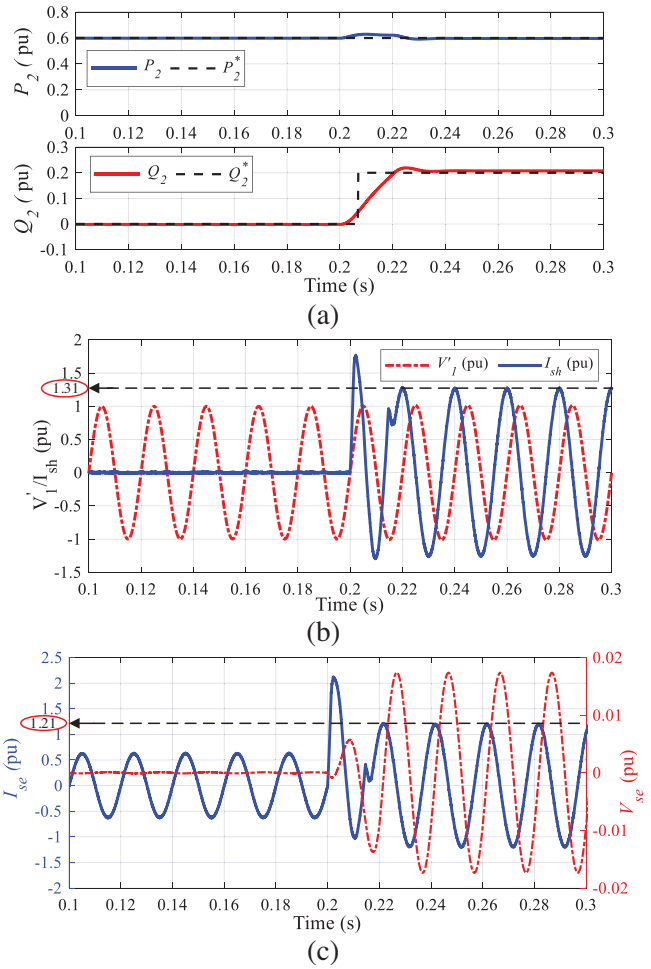

FIGURE 14 Simulation waveforms of case B; (a) P_2 and Q_2, (b) $\overline{V}_1{}'$ and $\overline{I}_{sh}$, and (c) $\overline{V}_{se}$ and $\overline{I}_{se}$

Figure 14a shows that Q_2 was increased from zero to 0.2 p.u. while P_2 was maintained constant at 0.6 p.u. in steady state. In response to this step change of reactive power, $|\bar{I}_{sh}|$ was increased to 1.31 p.u. and $|\bar{I}_{se}|$ to 1.21 p.u. in steady state as shown in Figure 14b,c. Both $|\bar{I}_{sh}|$ and $|\bar{I}_{se}|$ exceeded 1.0 p.u. These magnitudes match with case B in Section 3 and the phasor diagram in Figure 7a.

4.2.3 | Case C

Figure 15 shows the voltages and currents of the series and shunt converters when a step change of active and reactive power occurred at $t = 0.2$ s in response to changes in active and reactive power control signals. Before $t = 0.2$ s, the uncompensated active power was 0.2 p.u. and the uncompensated reactive power was zero.

Figure 15a shows that P_2 was increased from 0.2 to 0.6 p.u. and Q_2 was increased from zero to 0.2 p.u. in steady state. Figure 15b,c shows that current $|\bar{I}_{sh}|$ was increased to 0.64

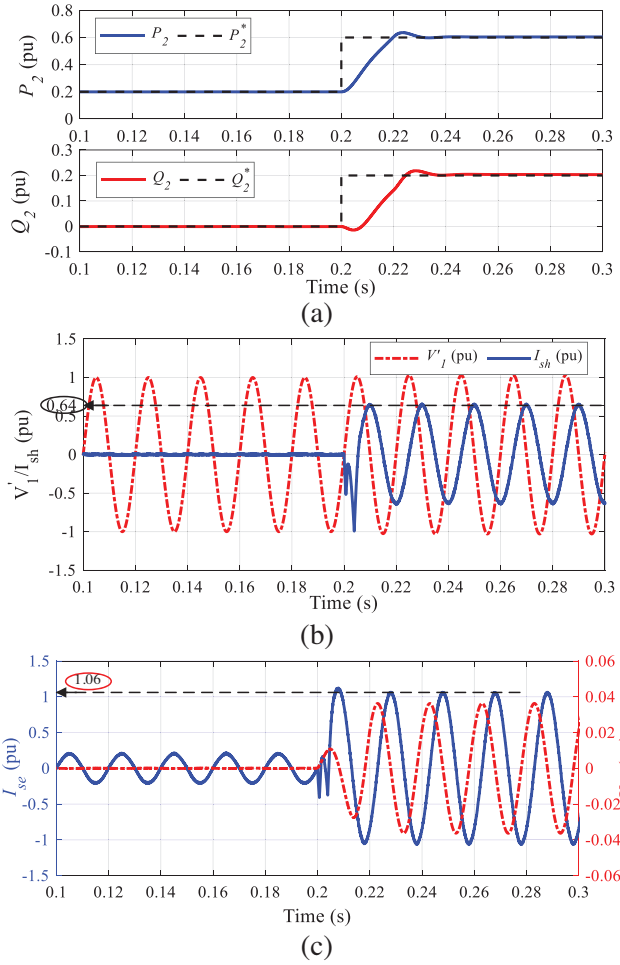

FIGURE 15 Simulation waveforms of case C; (a) P_2 and Q_2, (b) $\overline{V}_1'$ and $\overline{I}_{sh}$ and (c) $\overline{V}_{se}$ and $\overline{I}_{se}$

p.u., $|\overline{I}_{se}|$ was 1.06 p.u. Although $|\overline{I}_{sh}|$ was below 1.0 p.u., $|\overline{I}_{se}|$ exceeded 1.0 p.u. These results match with case C in Section 3 and the phasor diagram in Figure 7b.

5 | EXPERIMENTAL RESULTS

5.1 | Experimental equipment

A physical experiment was used to demonstrate the shunt current's magnitude of a transformer-less UPFC, as shown in Figure 16. It consists of:

1. An Imperix power electronic rig,
2. Two power amplifiers, and
3. A series impedance.

The Imperix power electronic rig has half-bridge modules that were connected to form the single-phase series converters and the three-phase shunt converter of a transformer-less UPFC. Two half-bridge modules were used to implement each two-level single-phase series converter and were directly connected to Busbar 1. Three half-bridge modules were used to implement a two-level three-phase shunt converter interfaced to busbar $\overline{V}_1'$ through a filter inductance L_{sh}.

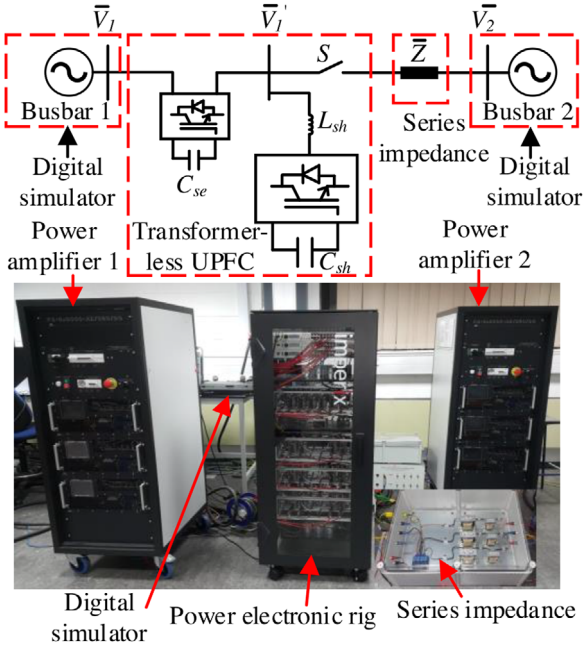

FIGURE 16 Physical set-up of the test system

TABLE 3 System parameters of the test setup

	Parameter	Value
AC network	Rated apparent power	0.75 kVA
	Phase voltage	$50\angle 0°$, 50 Hz
	Feeder's impedance	$0.68 + j\ 1.57\ \Omega$
PWM	Switching frequency	20 kHz
	Dead time band	1 μ s
Series converter	DC voltage, $V_{dc,se}$	20 V
	DC capacitance, C_{se}	750 μF
Shunt converter	DC voltage, $V_{dc,sh}$	150 V
	DC capacitance, C_{sh}	750 μF
	Filter inductance, L_{sh}	2.5 mH

Power amplifiers were used to emulate Busbar 1 and Busbar 2, and both were controlled using an OPAL-RT digital simulator. Series impedance represents the distribution feeder connecting Busbar 1 and Busbar 2. Table 3 shows the parameters of the test setup.

5.2 | Tests and results

The start-up of the experiment required starting the series converters and shunt converter and both are physically connected to the same point (i.e. busbar $\overline{V}_1'$). Then, synchronisation

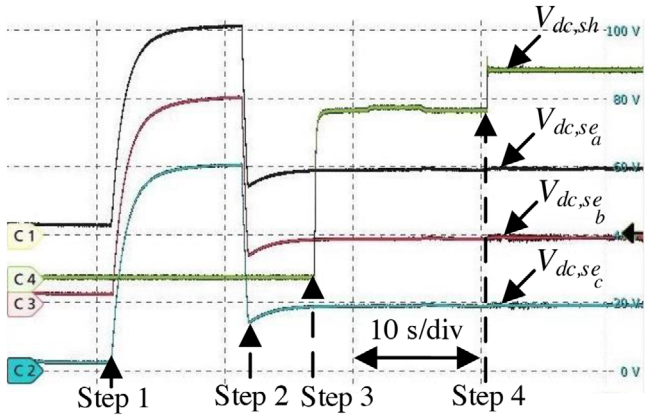

FIGURE 17 C1–C3) DC voltages of the three single-phase series converters with 20 V/div, and C4) the DC voltage of the shunt converter with 50 V/div

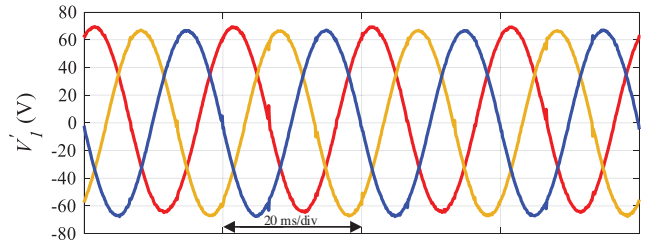

FIGURE 18 Experimental waveform of the phase voltage $\overline{V}_1'$

procedures were followed to connect Busbar 1 and Busbar 2. For simplicity, the experiment was conducted at low voltage.

Figure 17 shows the DC voltage across the DC buses of the series and shunt converters from start-up until steady state. In Step 1, the series converters were connected and charged through the anti-parallel diodes. In Step 2, the DC voltage controllers of the series converters were activated, and V_{dc,se_a}, V_{dc,se_b} and V_{dc,se_c} were maintained constant at 20 V. In Step 3, the shunt converter was connected and charged through the anti-parallel diodes. In Step 4, the DC voltage controller of the shunt converter was activated, and $V_{dc,sh}$ was maintained constant at 150 V. Figure 18 shows the experimental waveform of $\overline{V}_1'$ after closing the Switch "S".

Figure 19 shows the experimental results of the Transformerless UPFC in response to a control signal to step change the active power flow. Figure 19a shows the measured active power P_2 at Busbar 2. P_2 was increased from 0.36 to 0.8 p.u., while the reactive power Q_2 was maintained unchanged at 0.12 p.u. Figure 19b shows a small shunt current of approximately 0.63 A rms (i.e. 0.13 p.u.) provided by the shunt converter.

Figure 20 shows the experimental results of the transformerless UPFC in response to a control signal to step change the reactive power flow. Figure 20a shows that Q_2 was increased from 0.12 to 0.3 p.u. while P_2 was kept unchanged at 0.36 p.u. Figure 20b shows a large shunt current of 5.16 A rms (i.e. 1.03 p.u.).

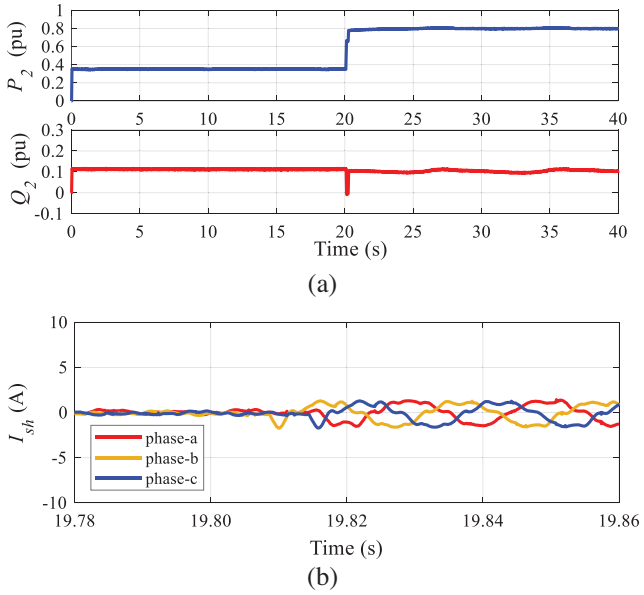

FIGURE 19 Experimental waveforms in response to step change of active power; (a) active and reactive power at Busbar 2, and (b) shunt current

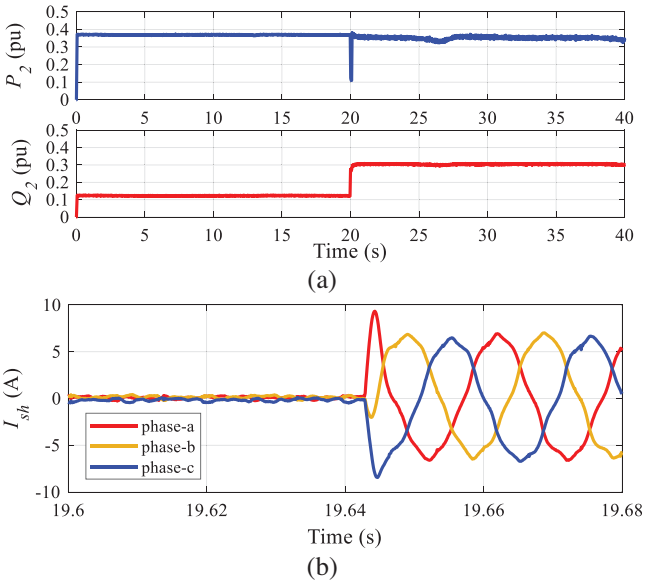

FIGURE 20 Experimental waveforms in response to step change of reactive power; (a) active and reactive power at Busbar 2, and (b) shunt current

It is worth noting that the lower voltage used in the experiment did not provide the same operating points as in the simulation results section. For example, the series converter controls the power flow by injecting series voltage up to 5 V (approximately 10% of the phase voltage). It was challenging to replicate the results in the simulation results section, considering the voltage drop of the wires, the IGBTs, and other passive components. However, the experiment highlights the most important findings of this work. These are; (1) a small shunt current when a transformer-less UPFC controls active power (see Figure 19b), and (2) a large shunt current

when a transformer-less UPFC controls reactive power (see Figure 20b).

The control schemes presented in Figures 11 and 12 provided the required power flow control of the transformer-less UPFC. Further analysis is required to optimise the operation of the transformer-less UPFC when connected to various types of AC systems [33].

6 | CONCLUSION

A transformer-less UPFC can provide power flow control in MV distribution networks using series and shunt converters that are not connected to a common DC-link and with complete removal of the interfacing transformers. Its operation relies on controlling the series and shunt converters together such that both converters exchange only reactive power with the AC network. The shunt current of the transformer-less UPFC was found to be small when it was used to control active power. In contrast, the use of the transformer-less UPFC to control reactive power required a large shunt current (i.e. > 1.0 p.u.). This makes a transformer-less UPFC a good choice for applications that require controlling active power. However, its ability to control reactive power is limited by the converters' current ratings.

AUTHOR CONTRIBUTIONS

Mohamed Abdelrahman: Conceptualization, Formal analysis, Investigation, Methodology, Validation, Visualization, Writing - original draft, Writing - review & editing. Sheng Wang: Conceptualization, Writing - review & editing. Wenlong Ming: Conceptualization, Project administration, Resources, Supervision, Writing - review & editing. Jianzhong Wu: Project administration, Supervision, Writing - review & editing. Nick Jenkins: Conceptualization, Investigation, Supervision, Writing - review & editing.

ACKNOWLEDGEMENTS

This work was supported in part by Newton-Mosharafa Fund and in part by the EPSRC Supergen Energy Networks Hub under grant EP/S00078X/1. The authors would like to thank Dr. Tibin Joseph for his help with the experimental work.

CONFLICT OF INTEREST

The authors declare no conflict of interest.

DATA AVAILABILITY STATEMENT

Data sharing not applicable to this article as no datasets were generated or analysed during the current study.

REFERENCES

1. Kroposki, B., Pink, C., Deblasio, R., Thomas, H., Simões, M., Sen, P.K.: Benefits of power electronic interfaces for distributed energy systems. IEEE Trans. Energy Convers. 25(3), 901–908 (2010). https://doi.org/10.1109/TEC.2010.2053975
2. Peng, F.Z.: Flexible AC transmission systems (FACTS) and resilient AC distribution systems (RACDS) in smart grid. Proc. IEEE. 105(11), 2099–2115 (2017). https://doi.org/10.1109/JPROC.2017.2714022
3. Long, C., Wu, J., Smith, K., Moon, A., Bryans, R., Yu, J.: MVDC link in a 33 kV distribution network. In: 24th International Conference & Exhibition on Electricity Distribution, Vol. 2017, Iss. 1, pp. 1308–1312. Cired, Open Acess Proc. J., Glasgow, (2017). https://doi.org/10.1049/oap-cired.2017.0168
4. Jupe, S.C.E., Hoda, S., King, J.E., Dale, D.A., Berry, J.: Controlling a 33 kV flexible power link in Gb's distribution network. IET Conference Publications. (2019), Coventry, UK. https://doi.org/10.1049/cp.2019.0021
5. Bottrell, N., Terry, S., Ash, N., Grella, L.: Active response to distribution network constraints. In: 25th International Conference on Electricity Distribution. Cired, Madrid (2019)
6. Bottrell, N., Lang, P., Green, T.: Algorithm for soft open points to solve thermal and voltage constraints in low-voltage distribution networks. In: 24th International Conference & Exhibition on Electricity Distribution. Cired, pp. 1567–1570, Glasgow, (2017). https://doi.org/10.1049/oap-cired.2017.0648
7. Frame, D., Hannon, M., Bell, K., McArthur, S.: Innovation in regulated electricity distribution networks: A review of the effectiveness of Great Britain's Low Carbon Networks Fund. Energy Policy 118, 121–132 (2018). https://doi.org/10.1016/j.enpol.2018.02.033
8. 'MV7000: Medium Voltage Drives, GE Power Conversion. https://www.gepowerconversion.com/product-solutions/medium-voltage-drives/mv7000 (Accessed on 16 Nov 2020)
9. Rodríguez, J., Bernet, S., Wu, B., Pontt, J.O., Kouro, S.: Multilevel voltage-source-converter topologies for industrial medium-voltage drives. IEEE Trans. Ind. Electron. 54(6), 2930–2945 (2007). https://doi.org/10.1109/TIE.2007.907044
10. Abdelrahman, M., Long, C., Wu, J., Jenkins, N.: Optimal operation of multi-terminal soft open point to increase hosting capacity of distributed generation in medium voltage networks. In: 53rd International Universities Power Engineering Conference (UPEC). Glasgow (2018). https://doi.org/10.1109/UPEC.2018.8541861
11. Bloemink, J., Green, T.C.: Benefits of distribution-level power electronics for supporting distributed generation growth. IEEE Trans. Power Delivery 28(2), 911–919 (2013). https://doi.org/10.1109/TPWRD.2012.2232313
12. Cao, W., Wu, J., Jenkins, N., Wang, C., Green, T.: Operating principle of Soft Open Points for electrical distribution network operation. Appl. Energy 164, 245–257 (2016). https://doi.org/10.1016/j.apenergy.2015.12.005
13. NERC. Short-Circuit Modeling and System Strength (2018). https://www.nerc.com/pa/RAPA/ra/Reliability%20Assessments%20DL/Short_Circuit_whitepaper_Final_1_26_18.pdf, (Accessed on 02 Nov 2020)
14. Gyugyi, L., Schauder, C.D., Williams, S.L., Rietman, T.R., Torgerson, D.R., Edris, A.: The unified power flow controller: A new approach to power transmission control. IEEE Trans. Power Delivery 10(2), 1085–1097 (1995). https://doi.org/10.1109/61.400878
15. 'UK Power Networks Innovation. Active Response. https://innovation.ukpowernetworks.co.uk/projects/active-response/ (Accessed on: 24 Oct 2021)
16. Jijun, Y., Haiqing, X., Jiankun, L.,Gang, C., Qun, L., Peng, L.: Unified power flow controller technology and application, pp. 43-79. Academic Press (2017). https://doi.org/10.1016/B978-0-12-813485-6.00003-0
17. Peng, F.Z., Liu, Y., Yang, S., Zhang, S., Gunasekaran, D., Karki, U.: Transformer-less unified power-flow controller using the cascade multilevel inverter. IEEE Trans. Power Electron. 31(8), 5461–5472 (2016). https://doi.org/10.1109/TPEL.2015.2497078
18. Gunasekaran, D., Yang, S., Peng, F.Z.: Fractionally rated transformer-less unified power flow controllers for interconnecting synchronous AC grids. In: Proceedings IEEE Applied Power Electronics Conference and Exposition - APEC. pp. 1795–1799. Charlott, NC, USA (2015). https://doi.org/10.1109/APEC.2015.7104590
19. Yang, S., Gunasekaran, D., Liu, Y., Karki, U., Peng, F.Z.: Application of transformer-less UPFC for interconnecting synchronous AC grids. In: IEEE Energy Conversion Congress and Exposition (ECCE). pp. 4993–4999. Montreal, QC, Canada (2015). https://doi.org/10.1109/ECCE.2015.7310364

20. Kaloudas, C.G., Ochoa, L.F., Marshall, B., Majithia, S., Fletcher, I.: Assessing the future trends of reactive power demand of distribution networks. IEEE Trans. Power Syst. 32(6), 4278–4288 (2017). https://doi.org/10.1109/TPWRS.2017.2665562
21. Abeysinghe, S.,Abdelrahman, M.A., Wickins, C., Wu, J., Jenkins, N.: Use of distributed generation to control reactive power at the transmission distribution interface. In: Proceedings of 2021 IEEE PES Innovative Smart Grid Technology. Espoo, Finland (2021). https://doi.org/10.1109/ISGTEUROPE52324.2021.9640219
22. Zheng, F., Zhang, S., Yang, S., Gunasekaran, D., Karki, U.: Transformerless unified power flow controller using the cascade multilevel inverter. In: International Power Electronics Conference (IPEC-Hiroshima - ECCE ASIA). pp. 1342–1349 (2014). https://doi.org/10.1109/IPEC.2014.6869760
23. Liu, Y., Yang, S., Wang, X., Gunasekaran, D., Karki, U., Peng, F.Z.: Application of transformer-less UPFC for interconnecting two synchronous AC grids with large phase difference. IEEE Trans. Power Electron. 31(9), 6092–6103 (2016). https://doi.org/10.1109/TPEL.2015.2500033
24. Koyama, Y., Nakazawa, Y., Mochikawa, H., Kuzumaki, A., Sano, K., Okada, N.: A transformerless 6.6-kV STATCOM based on a hybrid cascade multilevel converter using SiC devices. IEEE Trans. Power Electron. 33(9), 7411–7423 (2018). https://doi.org/10.1109/TPEL.2017.2770143
25. Balasubramaniam, S., Todeschini, G., Igic, P.: Voltage regulation in weak distribution grids using transformerless series compensators. In: IEEE Power Energy Society General Meeting, Atlanta, GA, USA (2019). https://doi.org/10.1109/PESGM40551.2019.8974055
26. Abdelrahman, M.A., Yang, P., Ming, W., Wu, J., Jenkins, N.: Modified unified power flow controller for medium voltage distribution networks. IET Gener. Transm. Distrib. 16, 3849–3859 (2022). https://doi.org/10.1049/GTD2.12567
27. Han, B., Bae, B., Baek, S., Jang, G.: New configuration of UPQC for medium-voltage application. IEEE Trans. Power Delivery 21(3), 1438–1444 (2006). https://doi.org/10.1109/TPWRD.2005.860235
28. Yang, S., Liu, Y., Wang, X., Gunasekaran, D., Karki, U., Peng, F.Z.: Modulation and control of transformerless UPFC. IEEE Trans. Power Electron. 31(2), 1050–1063 (2016). https://doi.org/10.1109/TPEL.2015.2416331
29. Bueno, E.J., Cobreces, S., Rodriguez, F.J., Espinosa, F., Alonso, M., Alcaraz, R.: Calculation of the DC-bus capacitors of the back-to-back NPC converters. In: 2006 12th International Power Electronics and Motion Control Conference. pp. 137–142. Portoroz, Slovenia (2009). https://doi.org/10.1109/EPEPEMC.2006.4778389
30. Neumayr, D., Bortis, D., Kolar, J.W.: The essence of the little box challenge-Part A: Key design challenges and solutions. CPSS Trans. Power Electron. Appl. 5(2), 158–179 (2020). https://doi.org/10.24295/CPSSTPEA.2020.00014
31. Domingues-Olavarria, G., Fyhr, P., Reinap, A., Andersson, M., Alakula, M.: From chip to converter: A complete cost model for power electronics converters. IEEE Trans. Power Electron. 32(11), 8681–8692 (2017). https://doi.org/10.1109/TPEL.2017.2651407
32. Wang, L.: Modeling and Control of Sustainable Power Systems : Towards Smarter and Greener Electric Grids. Springer, New York (2012)
33. Liu, Z., Guo, X.M.: Control strategy optimization of voltage source converter connected to various types of AC systems. J. Mod. Power Syst. Clean Energy 9(1), 77–84 (2021). https://doi.org/10.35833/MPCE.2020.000352

How to cite this article: Abdelrahman, M.A., Wang, S., Ming, W., Wu, J., Jenkins, N.: Transformer-less unified power flow controller in medium voltage distribution networks. IET Gener. Transm. Distrib. 1–13 (2023). https://doi.org/10.1049/gtd2.12730

APPENDIX

Derivation of Equation (8):

$$\left|\bar{I}_{se}\right|\underline{\left|\rho - 90^{\circ}\right.} = \left|\bar{I}\right|\underline{\left|\phi\right.} + \left|\bar{I}_{sh}\right|\underline{\left|\delta_s + 90\right.} \tag{A1}$$

Using Equation (A1), then

$$\left|\bar{I}_{sh}\right| = \frac{\left|\bar{I}\right| \cdot \cos(\phi) - \left|\bar{I}_{se}\right| \cdot \sin(\rho)}{\sin(\delta_s)} \tag{A2}$$

$$P_{sh} = 0, \textit{then } \textit{real}\left(\overline{V}'^{*}_{1} \cdot \bar{I}_{sh}\right) = 0 \tag{A3}$$

Using Equation (A3),

$$\left(\overline{V}_1 + \overline{V}_{se}\right) \cdot \left(\bar{I}_{se} - \bar{I}\right) = 0 \tag{A4}$$

From Equation (A4), the current $|\bar{I}_{se}|$is given in (A5).

$$\left|\bar{I}_{se}\right| = \frac{\left|\overline{V}_1\right| \cdot \left|\bar{I}\right| \cdot \cos(\phi) + \left|\overline{V}_{se}\right| \cdot \left|\bar{I}\right| \cdot \cos(\rho - \phi)}{\left|\overline{V}_1\right| \cdot \sin(\rho)} \tag{A5}$$

Substitute Equation (A5) into (A2),

$$\left|\bar{I}_{sh}\right| = -\frac{\left|\overline{V}_{se}\right| \cdot \left|\bar{I}\right| \cdot \cos(\rho - \phi)}{\left|\overline{V}_1\right| \cdot \sin(\delta_s)} \tag{A6}$$

Using $\overline{V}'_1 = \overline{V}_1 + \overline{V}_{se}$, then

$$\left|\overline{V}_1\right| = \left|\overline{V}_{se}\right| \left(\frac{\sin(\rho) \cdot \cos(\delta_s)}{\sin(\delta_s)} - \cos(\rho)\right) \tag{A7}$$

Substitute Equation (A7) into (A6)

$$\bar{I}_{sh} = \left|\bar{I}\right| \cdot \frac{\cos(\rho - \phi)}{\sin(\rho - \delta_s)} \underline{\left|(\delta_s - 90)^{\circ}\right.} \tag{A8}$$